Highly precise micro torsion angle detection by fringe array

Yang Gao (高 旸)*, Xingshu Wang (王省书), Chunsheng Hu (胡春生), Zongsheng Huang (黄宗升), and Dejun Zhan (战德军)

College of Opto-Electronic Science and Engineering, National University of Defense Technology, Changsha 410073, China

**Corresponding author: gaoyang_nudt@126.com*

Received April 3, 2014; accepted April 23, 2014; posted online July 18, 2014

Fringe array is proposed as the cooperated target in the precise torsion angle detection. The target fringe array image is generated according to the structure of the optical system, and the torsion angle detection algorithm is analyzed in response to the gray distribution of the image. The factors affecting the detection precision of the fringe torsion angle are analyzed theoretically and numerically. It indicates that the detection precision of the torsion angle is 1 angular second or even less, carefully selecting the detector array. Significantly, experiments are performed to demonstrate the precision and the results match well with the simulations.

OCIS codes: 040.1520, 110.3925.
doi: 10.3788/COL201412.080401.

Three dimensional (3D) angular deformations detection system is an important subsystem of the navigation system, and has been widely used in voyage, aeronautics, and astronautics[1]. With the development of the navigation technology, it is necessary to achieve a precision of several angular seconds in the 3D angular deformations detection system[2]. Although some detection methods have been proposed, such as inertia matching method[1−4], fiber Bragg gratings method[5−7], photogrammetry method[8−12], and optical collimated method[13−15], there is still not a precise and reliable detection method so far, for the complexity of the platform structure and the variability of the performance environment. Optical method is a superior method among the proposed methods, but it also has some limits. As is known, in an optical 3D angular deformations detection system, the pitching and yawing deformations are calculated by the movement of the cooperative target in the image, while the rolling deformation is calculated by the rotation of the target[13]. Therefore, it is difficult to detect the rolling deformation with the precision of several angular seconds in a digital image. To overcome this limit, many complex targets have been developed, such as moire fringe[14] and 3D target[8,9].

In this letter, we achieve precise torsion angle detection by fringe array. This target not only makes the optical structure simpler, but also makes the realization of practical detection easier, compared with the other complex targets proposed. This letter is organized as follows: Firstly, the fringe array image is generated in response to the optical system, to guarantee the uniformity of the simulation and the practical application. Secondly, the algorithm for detecting the torsion angle is proposed according to the gray distribution of the generated image. Thirdly, the fringe length and the torsion angle, the factors which impact the detection precision of the fringe angle, are analyzed in detail. Fourthly, it is demonstrated that high precision torsion angle detection can be achieved, with fringe array as the cooperated target. Finally, the experiments were performed to test the precision of this method.

As we know, when the fringe array image is transferred in the optical system, it will be impacted by spatial low-pass filtering, since the clear aperture of the optical system is limited. Therefore, the ideal gray distribution of the fringe edge obeys step distribution, and the practical gray distribution of the fringe edge obeys slowly changing distribution, rather than the commonly used Gaussian distribution. The ideal gray distribution of the fringe array can be expressed as

$$I_{\mathrm{I}}(x,y)=\sum_{i=1}^{n}\mathrm{rect}\left(\frac{x}{a}-x_i\right)=\begin{cases}1 & |x|\leqslant\dfrac{a}{2},y\leqslant\dfrac{b}{2}\\ 0 & \text{others}\end{cases}, \quad (1)$$

where a is the width of the fringe, b is the length of the fringe, x_i is the center of each fringe, and n is the fringe, number. Thus the spatial spectrum is the Fourier transform of the gray distribution:

$$G_{\mathrm{I}}(f_x,f_y)=F\{I_{\mathrm{I}}(x,y)\}. \quad (2)$$

Assuming that the optical system is noncoherent, the filter function can be expressed as

$$H(\rho)=\begin{cases}\dfrac{2}{\pi}\left[\arccos\left(\dfrac{\rho}{2\rho_0}\right)-\dfrac{\rho}{2\rho_0}\sqrt{1-\left(\dfrac{\rho}{2\rho_0}\right)^2}\right], & |\rho|\leqslant 2\rho_0\\ 0, & |\rho|>2\rho_0\end{cases}, \quad (3)$$

where ρ is defined by

$$\rho=\sqrt{f_x^2+f_y^2}, \quad (4)$$

and ρ_0 is the cutoff frequency of the optical system and defined by

$$\rho_0=\frac{D}{2\lambda z}, \quad (5)$$

herein D is the clear aperture of the optical system, λ and z are the wavelength and the optical wave propagating distance respectively.

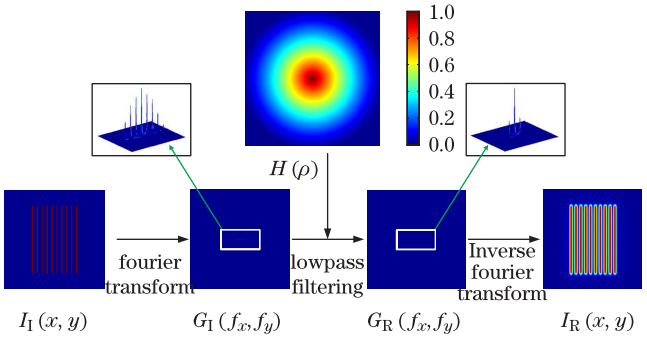

Fig. 1. Gray variation of the fringe array.

Therefore, the practice gray distribution is[16,17]

$$\begin{aligned} I_{\mathrm{R}}(x,y) &= F^{-1}\left\{G_{\mathrm{R}}(f_x,f_y)\right\} \\ &= F^{-1}\left\{G_{\mathrm{I}}(f_x,f_y)\cdot H(f_x,f_y)\right\}. \end{aligned} \tag{6}$$

The variation discussed above is shown in Fig. 1. Since the fringe array image is generated according to the parameters of the optical system, this generation method is more flexible than Gaussian function.

Common technologies in image procession, such as edge detection[18], Hough transform[19], and Radon transform[20], are not suitable for the precise fringe angle detection, not only because of the low calculating efficiency but also the limited precision. Our study indicates that the sub-pixel location algorithm can achieve the precise torsion angle detection in special conditions. The program of the fringe angle detection contains three steps. Firstly, there is a central point in every cross-section of one fringe, and its coordinate can be calculated by the subpixel location algorithm. Thus a coordinate array can be obtained from all the cross-sections in a fringe. Secondly, the fringe equation is found by the least square method, using the coordinate array obtained in the first step, and then the torsion angle can be calculated by the fringe slope. Assuming that the coordinate array is $(x_{0i}, y_{0i})(i = 1, 2, ..., n)$, the fringe is expressed as $y_{0i} = kx_{0i} + b$ where k, b are the parameters of the straight line, we obtain

$$\mathbf{BC} = \mathbf{Q}, \tag{7}$$

where

$$\mathbf{B} = \begin{bmatrix} x_{01} & 1 \\ x_{02} & 1 \\ \vdots & \vdots \\ x_{0n} & 1 \end{bmatrix}, \quad \mathbf{C} = \begin{bmatrix} k \\ b \end{bmatrix}, \quad \mathbf{Q} = \begin{bmatrix} y_{01} \\ y_{02} \\ \vdots \\ y_{0n} \end{bmatrix}.$$

The matrix $\mathbf{C}$ which contains the information of the fringe is given by

$$\mathbf{C} = (\mathbf{B}^{\mathrm{T}}\mathbf{B})^{-1}\mathbf{B}^{\mathrm{T}}\mathbf{Q}. \tag{8}$$

The torsion angle θ is given by

$$\theta = \mathrm{arctg}(k), \tag{9}$$

where k is the first element in $\mathbf{C}$. Thirdly, all the fringe torsion angles are calculated by the method introduced in the second step, and the torsion angle of the fringe array is the mean value of all the fringe torsion angles. In particular, it is almost impossible for the fringe cross-section to locate along the direction of the pixels, thus we cannot get the exact gray distribution on the cross-section, even by mature interpolation algorithm. To solve this problem, we search the central points on each section of the fringe along the direction of the pixels, for the symmetry of the fringe distribution.

As mentioned in the first step, gray centroid method and Gaussian fitting are both sub-pixel location algorithms for locating the central points in the fringe sections[21,22]. However, we find that Gaussian fitting, which always requires the gray values distribute as a Gaussian line, is not suitable for our requirement, because the gray values in the cross-section does not distribute as a Gaussian distribution line in our optical system. In the discussion above, we indicate that the gray distribution is impacted by the lowpass fitting effect and the fringe width. Considering that the cutoff frequency is fixed in the optical system, the fringe width becomes the core factor for the gray distribution in the image plane. Assuming that the wavelength is 680 nm, the clear aperture is 100 mm, and the propagating distance is 20 m, the cutoff frequency is 3.7×10^3 m^{-1} according to Eq. (4). When the pixel size is 5.5 μm, the gray distribution in the cross-section is shown in Fig. 2.

Figure 2 shows that the gray distributions of the fringe cross-section are symmetric and do not obey Gaussian distribution with the fringe widths of 20, 30, and 40 pixels. Therefore, we search the central point of the fringe by gray centroid method, which performs well when the distribution is symmetric. Thus the gray center of the fringe section can be given by

$$x_0 = \frac{\sum_{i=1}^{n} x_{\mathrm{s}i} I(x_{si})}{\sum_{i=1}^{n} I(x_{\mathrm{s}i})} \quad \text{or} \quad y_0 = \frac{\sum_{i=1}^{n} y_{\mathrm{s}i} I(y_{\mathrm{s}i})}{\sum_{i=1}^{n} I(y_{\mathrm{s}i})}, \tag{10}$$

where x_{si} (or y_{si}) is the coordinate of the pixel on the fringe section, $I(x_{si})$(or $I(y_{si})$) is the gray value of the pixel, and n is the total number of pixels on the fringe section. The former is performed when we search the center along the direction of x-axis and the latter is performed when we search the center along the direction of y-axis. To investigate whether this method is sensitive to the fringe width or not, we study the location errors of the gray centroid method and the results are shown in Fig. 3.

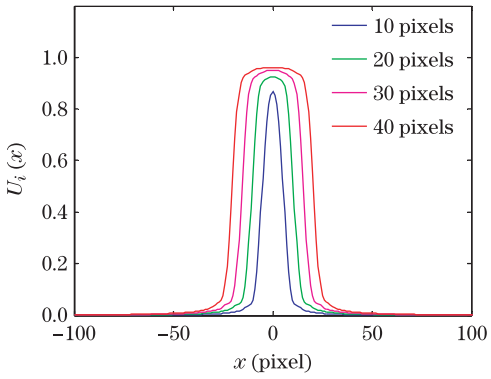

Fig. 2. Practice distribution of the fringe cross-section, with the ideal width of the fringe 10, 20, 30, and 40 pixels respectively.

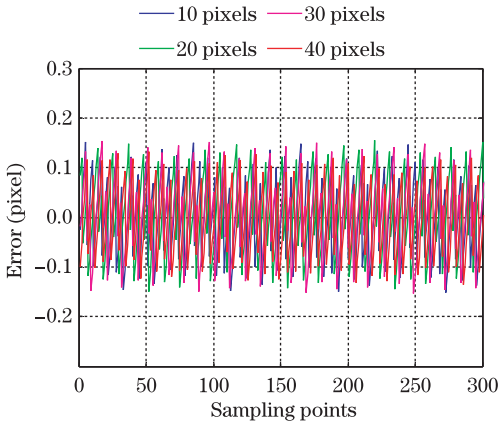

Fig. 3. Location errors in different fringe widths. The x-axis is the sampling points, and the y-axis is the location error.

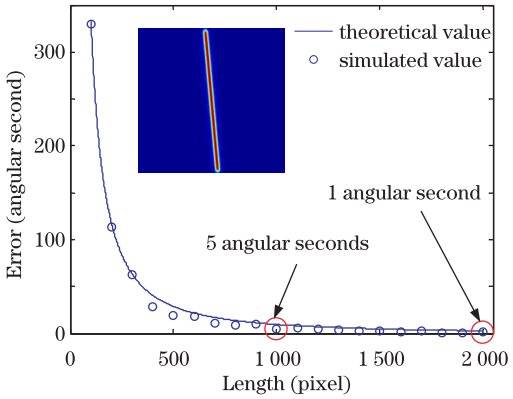

Fig. 4. Torsion angle errors of a single fringe. The solid line and the points denote the theoretical and simulated values respectively. The theoretical values is three times of the $\varepsilon_{\text{fringe}}$ standard deviation, and the simulated values show the calculation results by the algorithm mentioned above. According to the character of normal distribution, the theoretical value is larger than practical value, with the probability of 99.74%.

Figure 3 shows that the gray centroid method is not sensitive to the fringe width. Our further study shows that all the detection errors are less than 3 angular seconds, when the fringe length is 1000 pixels, the torsion angle is 5°, and the ideal width ranges from 10 to 40 pixels. In conclusion, the performance of the angle detection algorithm proposed is not sensitive to the fringe width, and the precision is at the magnitude of several angular seconds.

Although we have found an effective algorithm to detect the torsion angle effectively, it is not the only factor on the high precision torsion angle detection. The fringe length and the torsion angle itself play an important role too. According to the proposed algorithm, the torsion angle is calculated by the mean errors of the central point coordinates. Thus we can estimate the detection error from the location error of the algorithm. Assuming that the location error in a section is x_i, the mean location error x_{fringe} of a fringe can be expressed as

$$x_{\text{fringe}} = \frac{1}{n}\sum_{i=1}^{n} x_i, \tag{11}$$

where n is the length of the fringe. When x_i obeys normal distribution $N(\mu, \sigma^2)$, the distribution of x_{fringe} can be expressed as

$$x_{\text{fringe}} \sim N\left(\frac{\mu}{n}, \frac{\sigma^2}{n}\right). \tag{12}$$

The torsion angle error can be expressed as

$$\varepsilon_{\text{fringe}} = \text{arctg}\left(\frac{x_{\text{fringe}} - x'_{\text{fringe}}}{n}\right), \tag{13}$$

where x_{fringe} and x'_{fringe} are the two endpoints of the fringe. Thus the distribution of torsion angle error is

$$\varepsilon_{\text{fringe}} \sim N\left(0, \frac{2\sigma^2}{n^3}\right). \tag{14}$$

To certify the impact of the fringe length, numerical simulations are performed. When the torsion angle is 5°, the torsion angle error versus the fringe length is shown in Fig. 4.

Figure 4 shows that the theoretical value matches well with the simulated value. The longer the fringe is, the smaller the detection error will be. Particularly, when the length is 1000 pixels, the error will be less than 5 angular seconds and meets the requirement of precise torsion angle detection. Furthermore, the error is less than 1 angular second when the length is 2000 pixels. This result implies that precise torsion angle detection requires high resolution detector array, and the resolution should be at least one million pixels (1000×1000 (pixels)).

Torsion angle θ itself is also a factor affecting the precise detection. As shown in Fig. 5, we search the fringe sections along the direction of pixels.

In this way, the quantity of the sections as a function of θ can be expressed as

$$n = \begin{cases} \text{int}(N\cos\theta), & \theta \leqslant 45° \\ \text{int}(N\sin\theta), & \theta > 45°, \end{cases} \tag{15}$$

where N is the length of the fringe and int means the integer part. When the angle between the fringe and the direction of the pixels increases, the quantity of the sections involved in the calculation will decrease, and the detection error will increase as well. The detection error as a function of the torsion angle is shown in Fig. 6.

As shown in Fig. 6, the simulated result matches well with the theoretical values. It is demonstrated that the angle between the fringe and the direction of the detector array should be as small as possible, to achieve the precise detection.

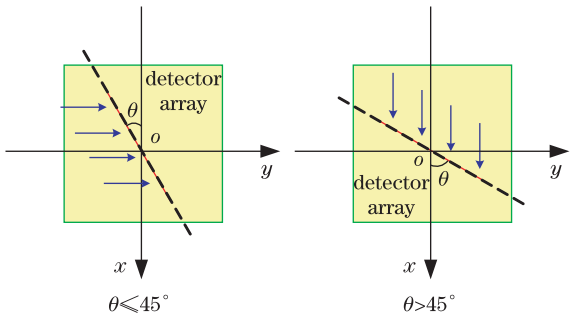

Fig. 5. Directions of the sections involved in calculation.

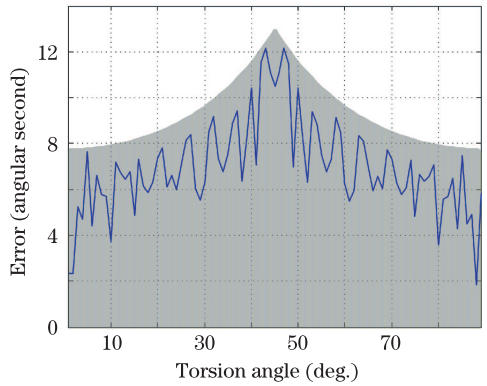

Fig. 6. Detection angle as a function of the torsion angle, with the fringe length 1000 pixels and the torsion angle 5°. The theoretical values denoted by the shadow area show three times of the $\varepsilon_{\text{fringe}}$ standard deviation, and the simulated values denoted by solid line show the calculation results by the algorithm proposed. According to the character of normal distribution, the solid line locates in the shadow area with probability of 99.74%. The fluctuation of the simulated values is induced by the discretization of the detector array.

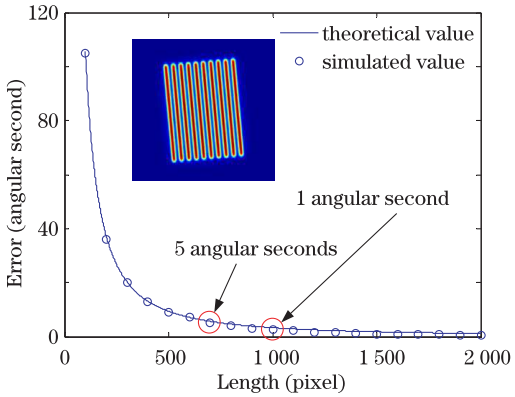

Fig. 7. Torsion angle errors of fringe array. The line and the points denote the theoretical and simulated values respectively. The theoretical values is three times of the $\varepsilon_{\text{array}}$ standard deviation, and the simulated values show the calculation results by the algorithm proposed. According to the character of normal distribution, the theoretical value is larger than practical value, with the probability of 99.74%.

Based on the discussion above, we detect the torsion angle by a fringe array, which is a novel cooperated target. Assuming that there are m fringes in the fringe array and the single fringe torsion angle error ε_j distributes as Eq. (14), the torsion angle error of the fringe array can be expressed as

$$\varepsilon_{\text{array}} = \frac{1}{m}\sum_{j=1}^{m}\varepsilon_j, \tag{16}$$

and its distribution is

$$\varepsilon_{\text{array}} \sim N\left(0, \frac{2\sigma^2}{mn^3}\right). \tag{17}$$

It is shown in Eq. (17) that the impact of m is weaker than n. When m=10 and the torsion angle is 5°, the torsion angle error as a function of the fringe length is shown in Fig. 7.

From Fig. 7, it is found that the theoretical value matches well with the simulated value. In Fig. 7, when the fringe length is 700 pixels, the error is less than 5 angular seconds, but this value is achieved when the fringe length is 1000 pixels with the single fringe target. Meanwhile, the error is less than 1 angular second with the fringe length of 1000 pixels in Fig. 7, and this result is achieved when the single target fringe length is 2000 pixels. It is demonstrated that the fringe array not only increases the detection precision but also reduces the requirement of the detector array resolution.

To demonstrate the precision of the fringe array torsion angle detection, an optical system is established as shown in Fig. 8. This system is composed of three parts: the projection unit, the receiving unit, and the autocollimator. In the projection unit, the fringe array target is installed in the focal plane of the collimated lens, with the clear aperture of 100 mm. The fringe array target is illuminated by a light-emitting diode (LED), with the wavelength of 680 nm. In the receiving unit, a charge coupled device (CCD), Prosilica GE1050, with 8-bit read out image and 1024×1024 (pixels) resolution, is installed in the focal plane of the convergent lens, whose clear aperture is the same as that of the collimated lens, thus the CCD captures the fringe array image projected by the projection unit. The torsion angle is calculated by the captured fringe array image, containing ten fringes with the length of 700 pixels. A mirror is installed in the receiving unit, and the optical axis of the mirror is perpendicular to that of the receiving unit. Thus the pitching angle of the mirror reflects the rolling deformation of the receiving unit. The autocollimator, TRIOPTICS TriAngle 1000−115 with the accuracy better than 0.2 angular second, is aligned in front of the mirror, to measure the practical pitching angle of the mirror. The errors of the fringe array detected torsion angle are given by the differences between the measured values by the fringe array and the ultrahigh precision autocollimator, ensuring the reliability of the experiment.

The experiments were performed in the hallway, with 20 m distance between the projection unit and the receiving unit. The optical path was protected by a pipe. The receiving unit was installed in a simulation platform to simulate the rolling deformation. The rolling deformation ranged from −150 to 150 angular seconds in our experiment, which is suitable to simulate the rolling deformation in a large structure. The rolling deformation was detected by the fringe array and autocollimator at the same time, and the experimental results are shown in Fig. 9.

It is shown in Fig. 9(a) that the torsion angles detected by the fringe array and the autocollimator match well

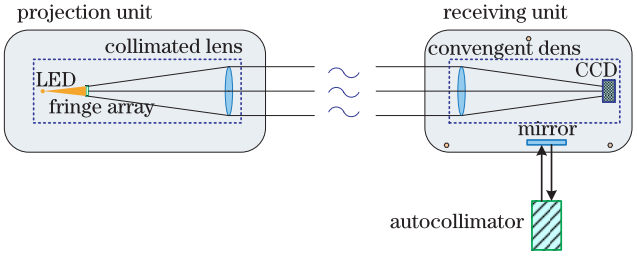

Fig. 8. Experimental measurement system.

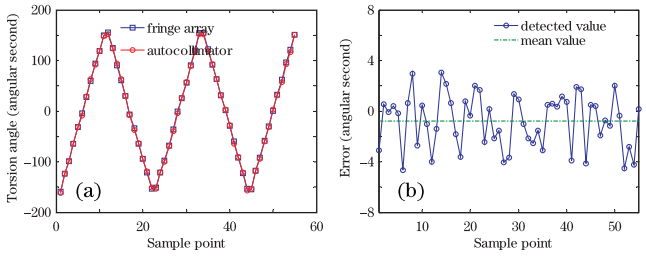

Fig. 9. The experimental results. (a) The torsion angle detected by fringe array and the autocollimator, (b) the torsion angle error detected by the fringe array. The detected value and the mean value of the errors are denoted by the blue line with circles and the green dash dotted line respectively.

with each other. From Fig. 9(b), it is demonstrated that the mean error and the root mean square of the torsion angle are −0.8 and 2.1 angular seconds respectively.

In conclusion, torsion angle is the most difficult to be precisely detected in the optical 3D angular deformations detection. Fringe array is proposed in this letter as the cooperated target to detect the torsion angle precisely. The structure of the optical system can be simplified by this target, and numerical simulation shows that the precision is as good as those of the complex moire fringe and 3D target. It is also demonstrated that the fringe array not only increases the precision, but also reduces the requirement of the detector array resolution, compared with a single fringe target. Experiments confirmed that this method achieved a high precision at the magnitude of angular second which matches well with the numerical simulations. Furthermore, the fringe array contains more information than a single fringe, thus the aberration impact may be controlled by the special algorithm, i.e. the torsion angle can be calculated by the weighted average of the torsion angles of all the fringes in the array, leading a new approach to the precise torsion angle detection.

This work was supported by the National Natural Science Foundation of China under Grant No. 61275002.

References

1. W. Wu, S. Chen, and S. Qin, IEEE Trans. Control. Syst. Technol. **21,** 1666 (2013).
2. G. Demoz and Y. Shao, IEEE Trans. Aerosp. Electron. Sy. **46,** 483 (2010).
3. D. Yang, S. Wang, H. Li, Z. Liu, and J. Zhang, J. Navig. **66,** 17 (2013).
4. L. Yuan and X. Cheng, Measurement **47,** 756 (2014).
5. R. A. Silva-Muñoz and R. A. Lopez-Anido, Compos. Struct. **89,** 224 (2009).
6. J. M. Nichols, M. Seaver, S. T. Trickey, K. Scandell, L. W. Salvino, and E. Aktas, J. Ship Ship Research **54,** 225 (2010).
7. Y. Qiu, Q. Wang, H. Zhao, J. Chen, and Y. Wang, J. Shanghai Jiaotong Univ. (Sci.) **18,** 129 (2013).
8. Q. Yu, G. Jiang, S. Fu, Z. Chao, Y. Shang, and X. Sun, Appl. Opt. **48,** 4683 (2009).
9. Z. Chao, Q. Yu, G. Jiang, and S. Fu, Appl. Opt. **49,** 5192 (2010).
10. Y. Shang, Q. Yu, Z. Yang, Z. Xu, and X. Zhang, Opt. Laser Eng. **54,** 247 (2014).
11. J. Yun, C. Gao, S. Zhu, C. Sun, H. He, L. Feng, L. Dong, and L. Liu, Chin. Opt. Lett. **10,** 121402 (2012).
12. Q. Nadeem and S. Na, Chin. Opt. Lett. **11,** 021402 (2013).
13. Y. Gao, X. Lu, X. Wang, C. Hu, and W. Wu, Proc. SPIE **8908,** 890805 (2013).
14. X. Liu, Y. Zhang, X. Feng, and Q. Wang, Appl. Mech. Mater. **344,** 93 (2013).
15. I. A. Konyakhin, T. V. Kopylova, A. I. Konyakhin, and A. A. Smekhov, Proc. SPIE **8759,** 87593E (2013).
16. Z. Zhou and L. Wang, in *Proceedings of IEEE Conference on Computer Science and Service System* 2885 (2011).
17. D. Cui, L. Ren, F. Shi, J. Shi, Y. Qian, H. Wang, and B. Chang, Chin. Opt. Lett. **10,** 060401 (2012).
18. G. Papari and N. Petkov, Image Vision Comput. **29,** 79 (2011).
19. O. J. Woodford, M. T. Pham, A. Maki, F. Perbet, and B. Stenger, Int. J. Comput. Vision. **106,** 332 (2014).
20. K. Jafari-Khouzani and H. Soltanian-Zadeh, IEEE Trans Pattern Anal. Machine Intell **27,** 1004 (2005).
21. H. C. van Assen, M. Egmont-Petersen, and J. H. C. Reiber, IEEE Trans. Image Process. **11,** 1379 (2002).
22. S. M. Anthony and S. Granick, Langmuir **25,** 8152 (2009).